Nuclear Engineering and Technology 52 (2020) 1545–1556

Contents lists available at ScienceDirect

Nuclear Engineering and Technology

journal homepage: www.elsevier.com/locate/net

Original Article

Dose coefficients of mesh-type ICRP reference computational phantoms for external exposures of neutrons, protons, and helium ions

Yeon Soo Yeom [a], Chansoo Choi [b], Haegin Han [b], Bangho Shin [b], Thang Tat Nguyen [c], Min Cheol Han [d], Chan Hyeong Kim [b, *], Choonsik Lee [a]

[a] Division of Cancer Epidemiology and Genetics, National Cancer Institute, National Institutes of Health, Rockville, MD, 20850, USA
[b] Department of Nuclear Engineering, Hanyang University, Seoul, 04763, South Korea
[c] School of Nuclear Engineering and Environmental Physics, Hanoi University of Science and Technology, 1 Dai Co Viet Road, Hai Ba Trung District, Hanoi, Viet Nam
[d] Department of Radiation Oncology, Yonsei University College of Medicine, Seoul, 03722, South Korea

ARTICLE INFO

Article history:
Received 20 November 2019
Accepted 20 December 2019
Available online 25 December 2019

Keywords:
ICRP reference phantom
Mesh
Dose coefficient
Neutrons
Protons
Helium ions

ABSTRACT

Recently, the International Commission on Radiological Protection (ICRP) has developed the Mesh-type Reference Computational Phantoms (MRCPs) for adult male and female to overcome the limitations of the current Voxel-type Reference Computational Phantoms (VRCPs) described in ICRP *Publication* 110 due to the limited voxel resolutions and the nature of voxel geometry. In our previous study, the MRCPs were used to calculate the dose coefficients (DCs) for idealized external exposures of photons and electrons. The present study is an extension of the previous study to include three additional particles (i.e., neutrons, protons, and helium ions) into the DC library by conducting Monte Carlo radiation transport simulations with the Geant4 code. The calculated MRCP DCs were compared with the reference DCs of ICRP *Publication* 116 which are based on the VRCPs, to appreciate the impact of the new reference phantoms on the DC values. We found that the MRCP DCs of organ/tissue doses and effective doses were generally similar to the ICRP-116 DCs for neutrons, whereas there were significant DC differences up to several orders of magnitude for protons and helium ions due mainly to the improved representation of the detailed anatomical structures in the MRCPs over the VRCPs.

1. Introduction

Recently, the Task Group 103 of the International Commission on Radiological Protection (ICRP) has developed the Mesh-type Reference Computational Phantoms (MRCPs) for adult male and female in order to overcome several inherent limitations of the Voxel-type Reference Computational Phantoms (VRCPs) described in ICRP *Publication* 110 [1] due to the limited voxel resolutions and the nature of the voxel geometry [2]. The MRCPs now include micron-scale radiosensitive target and source regions of the respiratory and alimentary tract systems, skin, lens of the eyes, and urinary bladder [3–6], which could not be defined in the ICRP-110 VRCPs composed of millimetre-scale voxels. As a surrogate of the radiosensitive regions, the entire organ/tissue volume of the VRCPs was used in the calculation of the current reference dose coefficients (DCs) for external exposures provided in ICRP *Publication* 116 [5].

In our previous study [7], the MRCPs were used to calculate DCs for photons and electrons, which were then compared with the ICRP-116 DCs based on the VRCPs to investigate the impact of the new reference phantoms on DC calculations. The results showed that the MRCP-based DCs overall agree with the VRCP-based DCs for photons. The percent DC differences for effective dose between MRCPs and VRCPs are less than 5% for most cases. For electrons, on the other hand, significant DC differences up to several orders of magnitude were observed for superficial organs/tissues (e.g., skin and breasts) and skeletal tissues, which is due to the improved representation of the tissue structures in the MRCPs. In addition to the organ/tissue doses, significant differences in effective dose were observed for electron energies less than 1 MeV, where the

* Corresponding author.
E-mail address: chkim@hanyang.ac.kr (C.H. Kim).

https://doi.org/10.1016/j.net.2019.12.020

VRCP-based DCs underestimate the MRCP-based effective doses (assumed to be more accurate) by a factor of ~10 at 0.1 MeV. It is now important to extend the previous study to evaluate the impact of the MRCPs on DC calculations with respect to other radiation particles.

In the present study, we established a comprehensive set of MRCP-based DCs for three particles, i.e., neutrons, protons, and helium ions, by conducting Monte Carlo radiation transport simulations. The dataset includes dose coefficients for organ/tissue-averaged absorbed dose (DC_T's) to 30 organs and tissues and for effective dose (DC_E's) with respect to the irradiation geometries and energies used in ICRP *Publication* 116 [5]. The MRCP-based DCs were finally compared with the ICRP-116 DCs to observe dosimetric impact of the MRCPs against the VRCPs.

2. Material and methods

The adult male and female MRCPs (see Fig. 1) were implemented in the Geant4 Monte Carlo code (ver. 10.04) [8] for the calculations of DCs following the implementation method described in Yeom et al. [9]. The phantoms were assumed to be located in a vacuum and irradiated by mono-energetic broad parallel beams. As considered in ICRP *Publication* 116 [5], six irradiation geometries, i.e., antero-posterior (AP), postero-anterior (PA), left-lateral (LLAT), right-lateral (RLAT), rotational (ROT), and isotropic (ISO), were used for neutrons and protons, and three irradiation geometries, i.e., AP, PA, and ISO, were used for helium ions. The energy bins were also selected corresponding to those used in ICRP *Publication* 116: 10^{-9}–10^{4} MeV for neutrons, 1–10^{4} MeV for protons, and 1–10^{5} MeV/u for helium ions. Parallel beams were simulated by creating a 2-m-diameter disk source that uniformly emits particles in its normal direction, incident to the whole body of the phantoms, by using the approach described in Yeom et al. [7].

DC_T, organ/tissue-averaged absorbed dose per fluence (pGy cm^2), for all organs/tissues required for effective dose calculation [10] and the lens of the eyes were directly calculated from the MRCPs via the *G4PSEnergyDeposit* class except the skeletal tissues (red bone marrow (RBM) and endosteum). The absorbed doses of the RBM and endosteum, the microscopic structures of which were not explicitly modelled in the skeletons of the MRCPs as well as the VRCPs [11], were approximated as the mass-weighted average of the dose delivered to the regional spongiosa and medullary cavity following the approach used for the ICRP-116 DCs [5]. The calculated DC_T's were then used to derive DC_E, effective dose per fluence (pSv cm^2) from the following equation:

$$DC_E = \sum_T w_T \sum_R w_R \left(\frac{DC_{T,R}^{Male} + DC_{T,R}^{Female}}{2} \right) \quad (1)$$

where $DC_{T,R}$ is the dose coefficient for the organ/tissue T and radiation R, w_T is the tissue-weighting factor, and w_R is the radiation-weighting factor defined in ICRP *Publication* 103 [10].

The physics libraries, *G4EmLivermoverPhysics* and *QGSP_BIC_HP*, were used to transport all the particles with all energy bins except for the neutrons below 20 MeV for which the physics models and cross-section data were summarized in Table 1. The thermal neutron scattering treatment S(alpha, beta) for hydrogen in light water at 300K was activated to take the thermal vibration of molecules into account. The range value of 1 μm for the secondary production cut was set to all the particles. The number of primary particles varied from 10^{8} to 10^{10} depending on the particles and energies to keep statistical relative errors for all the calculated DC_E's below 5% and for the majority of the calculated DC_T's below 1%. The simulations were performed on Biowulf, the National Institutes of Health's high-performance Linux computing cluster (http://hpc.nih.gov).

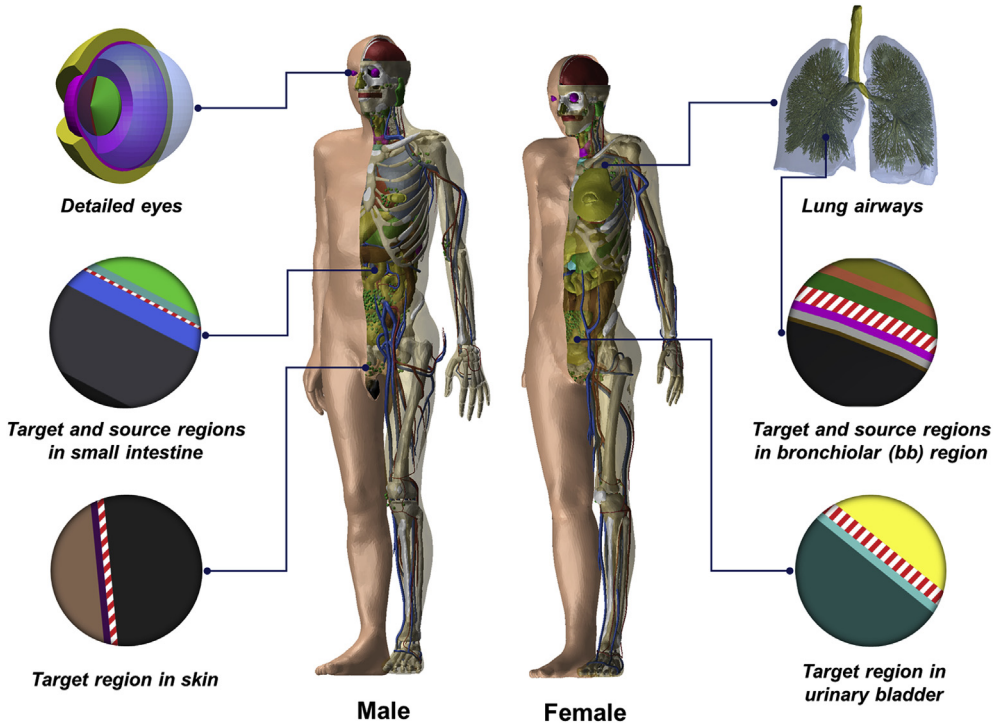

Fig. 1. Adult male and female mesh-type ICRP reference computational phantoms. Micron-scale radiosensitive regions of major organs and tissues are visualized on the left and right of the phantoms.

Table 1
Physics models and cross sections used in Geant4 for simulation of neutrons below 20 MeV.

Process category	Models	Cross sections
hadElastic	NeutronHPThermal-Scattering (0–4 eV) NeutronHPElastic (4 eV–20 MeV)	NeutronHPThermal-ScatteringData (0–4 eV) NeutronHPElasticXS (4 eV–20 MeV)
neutronInelastic	ParticleHPInelastic	NeutronHPInelasticXS
nCapture	NeutronHPCaptureXS	NeutronHPCaptureXS
nFission	NeutronHPFission	NeutronHPFissionXS

It should be noted that the DC_T's for the organs and tissues that include the radiosensitive regions (i.e., the extrathoracic (ET) region, lungs, oesophagus, stomach, small and large intestines, skin, urinary bladder, and eye lens) in the MRCPs was calculated by averaging absorbed dose over the sensitive organ/tissue volume. An additional set of DC_T's for these organs and tissues was calculated by using the entire organ/tissue regions as a surrogate of the sensitive regions, i.e., by averaging absorbed dose over the entire organ/tissue volume. Besides, an additional set of DC_E's was produced by applying the entire-region based DC_T's. The entire-region based DCs were compared with the sensitive-region based DCs to investigate dosimetric impact of the detailed modelling of the sensitive regions in the MRCPs.

3. Results and discussion

3.1. Dose coefficients for neutrons, protons, and helium ions

A comprehensive DCs for the MRCPs for external exposures of neutrons, protons, and helium ions were established in the present study. The data includes DC_T's, organ dose per fluence (pGy cm^2) for 30 organs/tissues (i.e., RBM, colon, lung, stomach, breast, testes, ovaries, urinary bladder, oesophagus, liver, thyroid, endosteum, brain, salivary glands, skin, adrenals, ET region, gall bladder, heart, kidneys, lymphatic nodes, muscle, oral mucosa, pancreas, prostate, small intestine, spleen, thymus, uterus, and eye lens) and DC_E's, effective dose per fluence (pSv cm^2). The neutron DCs were obtained for 68 energy values ranging from 10^{-9} to 10^4 MeV and six irradiation geometries (AP, PA, LLAT, RLAT, ROT, and ISO). The proton DCs were obtained for 33 energy values ranging from 1 to 10^4 MeV and six irradiation geometries (AP, PA, LLAT, RLAT, ROT, and ISO). The helium ion DCs were obtained for 24 energy values

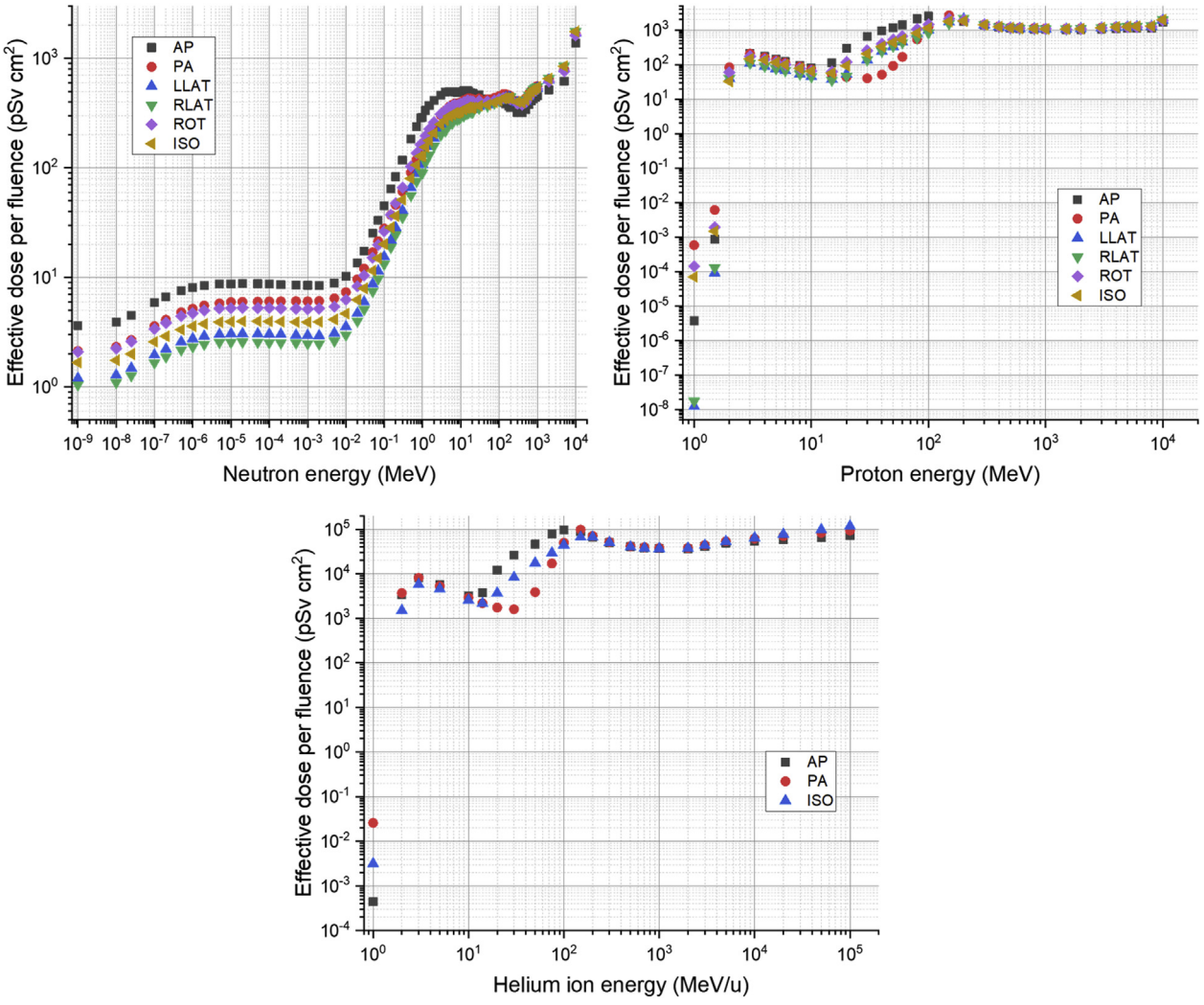

Fig. 2. Effective dose per fluence (pSv cm^2) calculated with MRCPs and Geant4 code for neutrons (upper left), protons (upper right), and helium ions (lower).

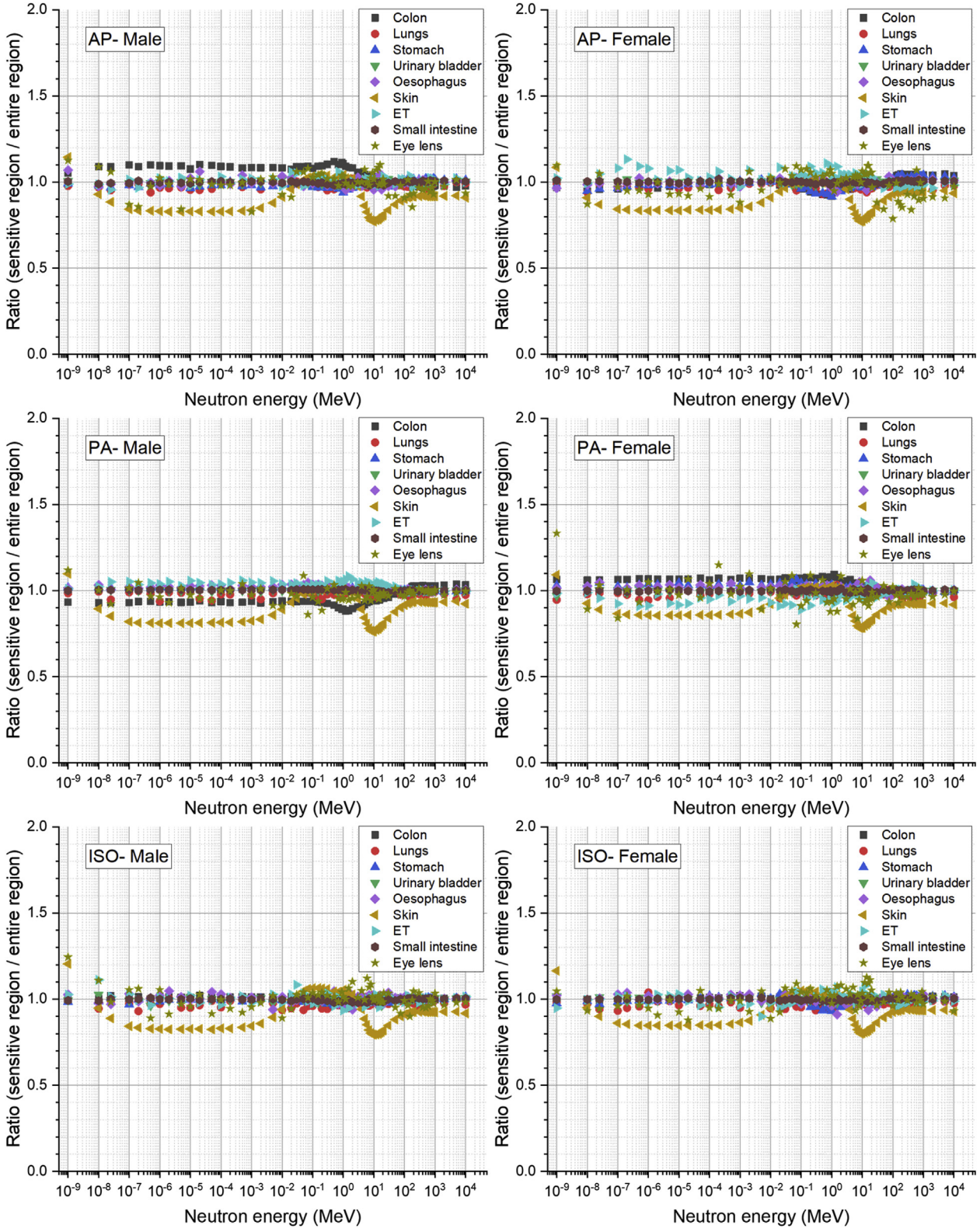

Fig. 3. Ratios of DC_T's based on sensitive region to the values based on entire region for colon, lungs, stomach, urinary bladder, oesophagus, skin, ET region, small intestine, and eye lens of male (left) and female (right) MRCPs for neutrons in AP, PA, and ISO geometries.

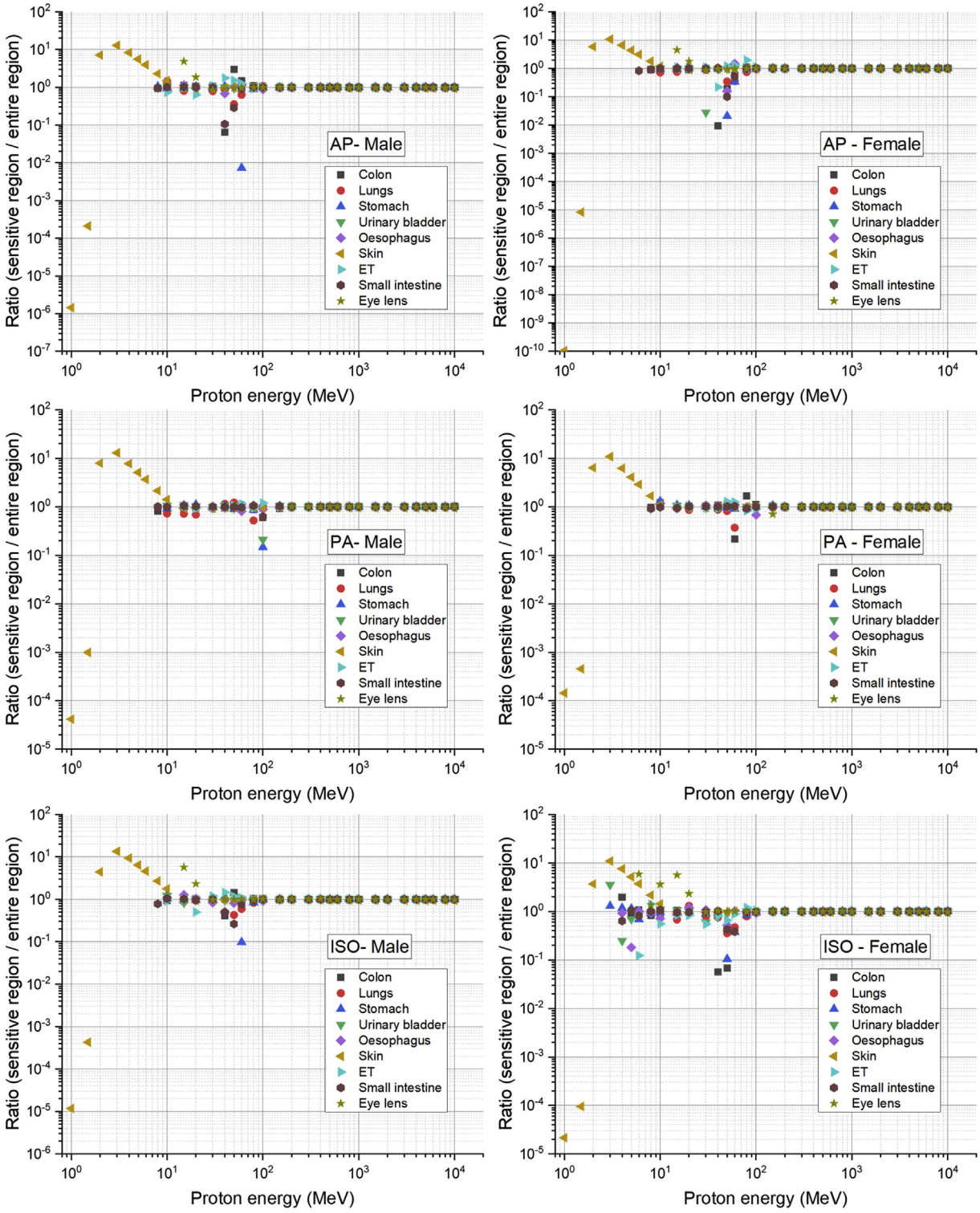

Fig. 4. Ratios of DC_T's based on sensitive region to the values based on entire region for colon, lungs, stomach, urinary bladder, oesophagus, skin, ET region, small intestine, and eye lens of male (left) and female (right) MRCPs for protons in AP, PA, and ISO geometries.

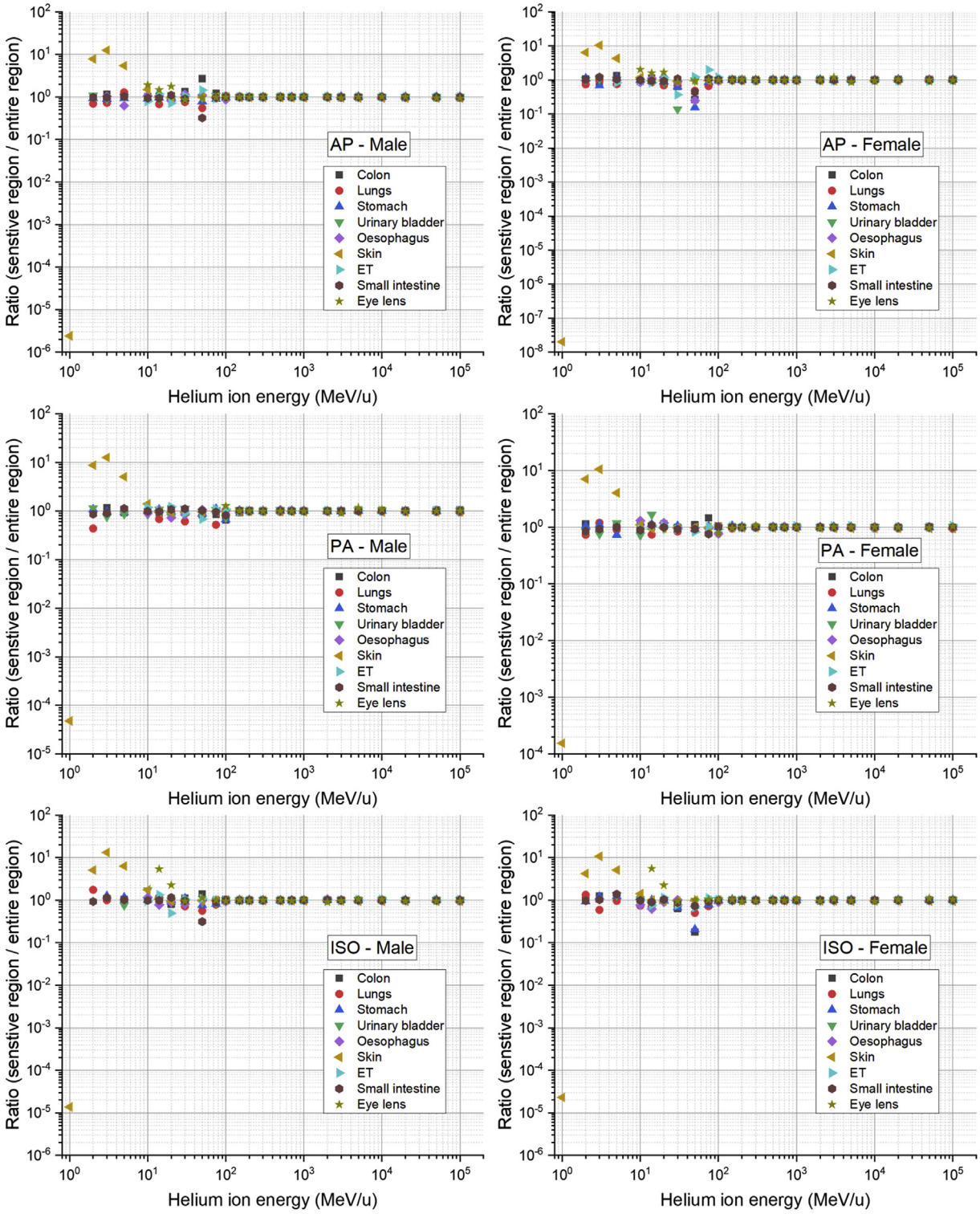

Fig. 5. Ratios of DC_T's based on sensitive region to the values based on entire region for colon, lungs, stomach, urinary bladder, oesophagus, skin, ET region, small intestine, and eye lens of male (left) and female (right) MRCPs for helium ions in AP, PA, and ISO geometries.

ranging from 1 to 10^5 MeV/u and three irradiation geometries (AP, PA, and ISO). The numerical values of all the DCs are tabulated in the supplementary data tables available online. Fig. 2 plots the DC_E's for all the particles and irradiation geometries.

3.2. Dosimetric impact of micron-scale radiosensitive regions

Fig. 3 shows the ratios of the radiosensitive-region based DC_T's to the entire-region based DC_T's for neutrons in the AP, PA, and ISO geometries. The ratios are mostly close to unity (0.9–1.1) over the entire energy region, which indicates that the influence of the detailed modelling of the sensitive regions on organ/tissue doses is generally not significant. Relatively large deviations from unity can be seen for the skin but the ratios are still within a range from 0.8 to 1.2 for most energies. Fig. 4 shows the ratios for protons. At energies >100 MeV, the ratios for all the organs and tissues are close to unity (0.9–1.1), while large deviations from unity can be seen at lower energies by up to several orders of magnitude. At energies <10 MeV, the skin shows notably large deviations in all the geometries. The ratios at energies ≤1.5 MeV are lower than unity, with a minimum of ~10^{-10} for the female phantom at 1 MeV in the AP geometry. This means that the entire-region based skin doses significantly overestimate the sensitive-region based values. At higher energies, on the other hand, the sensitive-region based skin doses are significantly underestimated by up to about an order of magnitude at 3 MeV. Fig. 5 shows the ratios for helium ions, showing the trend similar to those for protons. At energies >100 MeV/u, the ratios are close to unity (mostly between 0.9 and 1.1) whereas at lower energies, large deviations from unity by up to several orders of magnitude are observed especially for the skin.

Fig. 6 shows the ratios of the sensitive-region based DC_E's to the entire-region based DC_E's. For neutrons, the ratios are very close to unity for all the energies and geometries (mostly between 0.95 and 1.05), which means that the influence of the detailed modelling of the sensitive regions on effective dose is negligible. For protons, the ratios are also close to unity at energies >10 MeV but significantly deviate from unity at lower energies. At energies ≤1.5 MeV, the ratios are lower than unity by about three to eight orders of magnitude; that is, the effective doses from the entire volume models significantly overestimate the values from the detailed organ models. At higher energies, on the other hand, the entire-region based effective doses significantly underestimate the detailed model-based effective doses by up to about an order of magnitude.

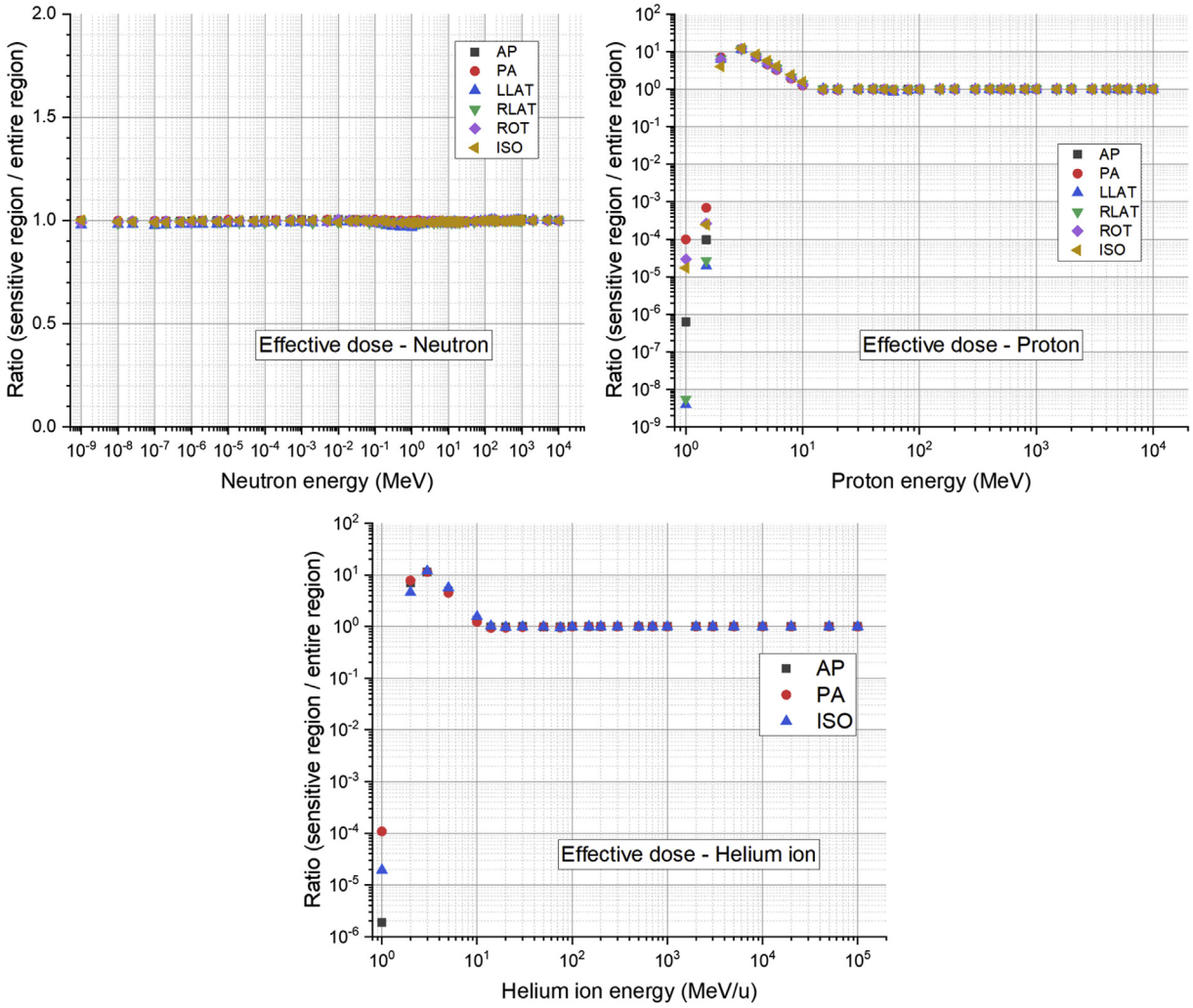

Fig. 6. Ratios of DC_E's of MRCPs based on sensitive region to the values based on entire region for neutrons (upper left), protons (upper right), and helium ions (lower).

These significant differences in effective doses are influenced mainly by the skin dose differences described above. Note that despite the small tissue-weighing factor (= 0.01) [10] the skin doses mainly contribute to effective doses because these low-energy protons (<10 MeV) deposit most of their energies to the skin. For helium ions, the general trend is very similar to that for protons; that is, the ratios are close to unity over the entire energy bins except for the low energies (<10 MeV/u) where the ratios significantly deviate from unity by up to about six orders of magnitude. These differences are again mainly due to the skin dose differences.

3.3. Comparison with ICRP publication 116 dose coefficients

3.3.1. Organ/tissue doses coefficients

Fig. 7 shows the ratios of the MRCP DC_T's to the ICRP-116 DC_T's for 15 organs/tissues (RBM, colon, lungs, stomach, breasts, remainder tissues, gonads, urinary bladder, oesophagus, liver, thyroid, endosteum, brain, salivary glands, and skin) for neutrons in the ISO geometry. The ratios for all the organs and tissues are generally within a range from 0.8 to 1.2 across the entire energy bins. Relatively large deviations from unity are observed at the lowest and highest energies where the ratios are mostly lower than 1.5. These differences between the MRCP DC_T's and ICRP-116 DC_T's, however, are not due to the difference in phantom geometry or material composition, but due mainly to the difference in the cross-section data or physics models employed in different Monte Carlo codes. Note that the MRCP DCs were calculated with the Geant4 code, while the ICRP-116 DCs were calculated with four different codes (MCNPX, PHITS, FLUKA, and Geant4) and went through averaging and smoothing processes [5]. Although not presented in this paper, the MRCP DC_T's were also compared with the values calculated with the VRCPs and the Geant4 code, observing the differences were less than 5% for most cases.

Fig. 8 shows the ratios of the MRCP DC_T's to the ICRP-116 DC_T's for protons. At energies >100 MeV, the ratios tend to be close to unity (mostly between 0.9 and 1.1). At lower energies, on the other hand, large deviations from unity are frequently observed by up to several orders of magnitude, which are mainly due to the improvement of the MRCPs compared to the VRCPs. For the skin, as an example, the ratios at energies <10 MeV are significantly different from unity, and almost identical to the ratios of the MRCP sensitive-region based skin

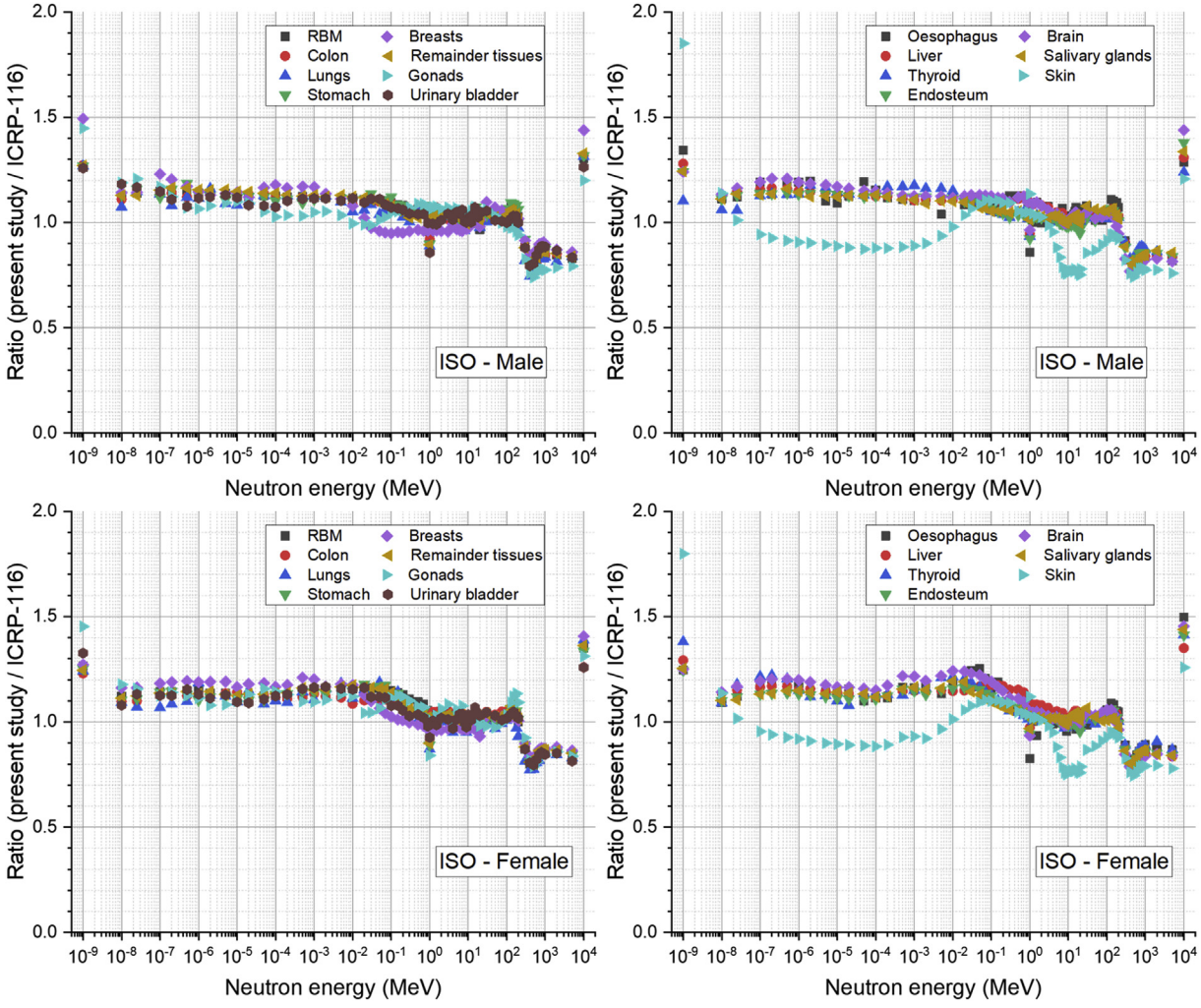

Fig. 7. Ratios of MRCP DC_T's calculated in present study to ICRP-116 DC_T's [5] for RBM, colon, lungs, stomach, breasts, remainder tissues, gonads, urinary bladder, oesophagus, liver, thyroid, endosteum, brain, salivary glands, and skin for neutrons in ISO geometry.

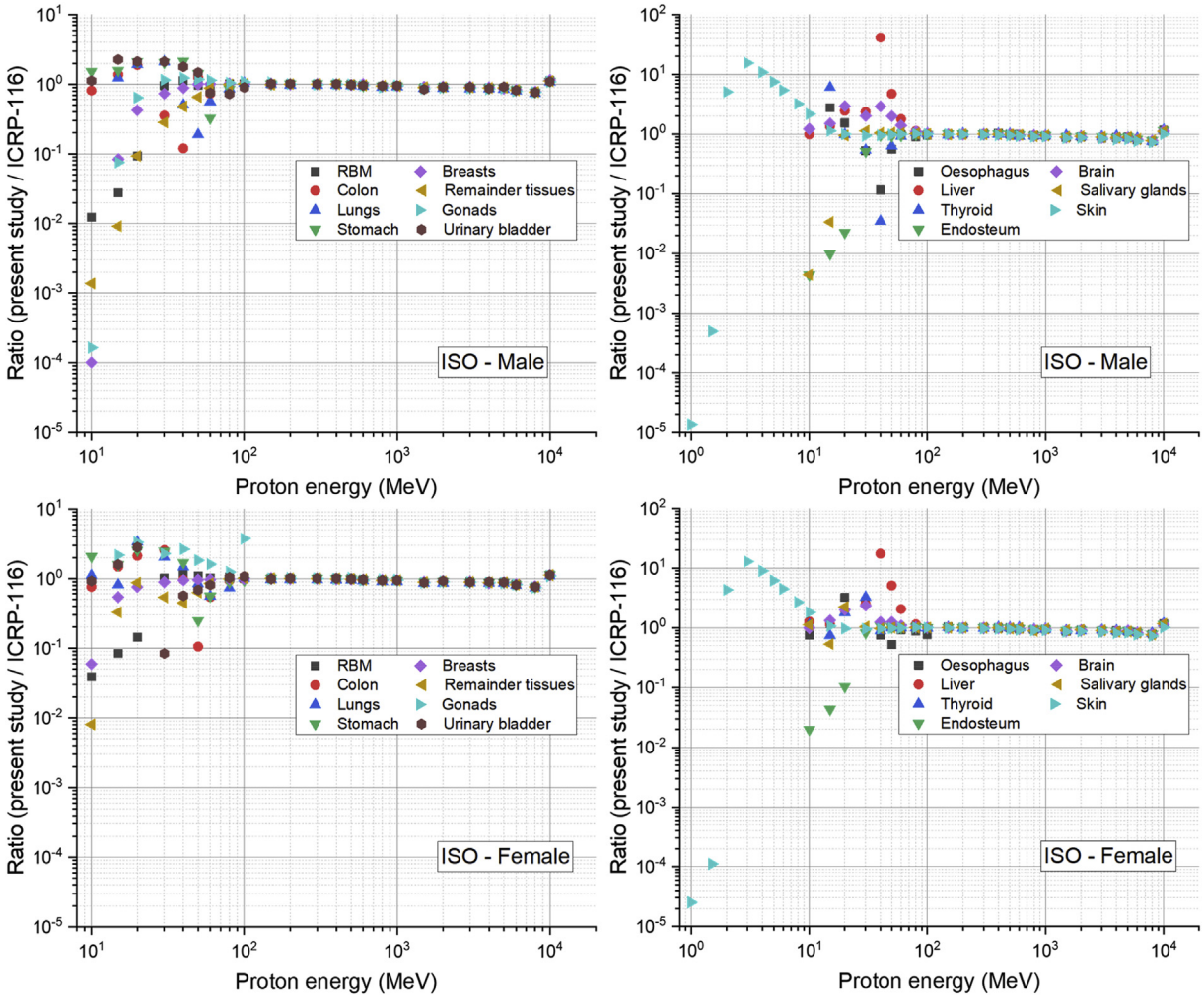

Fig. 8. Ratios of MRCP DC_T's calculated in present study to ICRP-116 DC_T's [5] for RBM, colon, lungs, stomach, breasts, remainder tissues, gonads, urinary bladder, oesophagus, liver, thyroid, endosteum, brain, salivary glands, and skin for protons in ISO geometry.

DCs to the MRCP entire-region based skin DCs as shown in Fig. 4. This means that the deviations from the ICRP-116 skin DCs are mainly due to the skin sensitive region in the MRCPs. Other superficial organs/tissues (breasts, gonads, and salivary glands) show the ratios tend to be significantly lower than unity; that is, the MRCP DCs are significantly lower than the ICRP-116 values. The differences are attributed to the improved representation of the skin in the MRCPs, i.e., eliminating the discontinuous region of the skin in the VRCPs due to the limited voxel resolutions. Protons through the discontinuous skin region in the VRCPs directly deposited energies to the superficial organs/tissues, the absorbed doses to which were eventually overestimated. This limitation also resulted in the significant overestimation to the ICRP-116 DCs of the remainder tissues including some organs/tissues (e.g., muscle and lymphatic nodes) directly exposed to the protons through the discontinuous skin region. It should be noted that acknowledging the skin limitation of the VRCPs, the ICRP-116 DCs for all organs and tissues except for skin were set to zero for proton energies <10 MeV [5]; nevertheless, the ICRP-116 DCs at higher energies still significantly overestimate doses to the superficial organs/tissues and some of the remainder tissues. In addition, the skeletal tissues (RBM and endosteum) show the MRCP DCs are significantly lower than the ICRP-116 DCs, which are due to the improved representation not only of the skin but also of the cortical bone in the MRCPs. In the VRCPs, the cortical bone in thin structure is discontinuously represented like the skin and therefore protons directly deposited energies to the inner skeletal structures (i.e., spongiosa and medullary-cavity regions). This limitation is fully eliminated in the MRCPs [11]. The results for helium ions in Fig. 9 show the general trend is similar to that for protons. The MRCP DCs tend to be close to the ICRP-116 DCs at energies >100 MeV/u but significantly different at lower energies, which are again due mainly to the improvements of the MRCPs.

3.3.2. *Effective dose coefficients*

Fig. 10 shows the ratios of the MRCP DC_E's to the ICRP-116 DC_E's for all the particles and irradiation geometries considered in the present study. For neutrons, the ratios tend to be

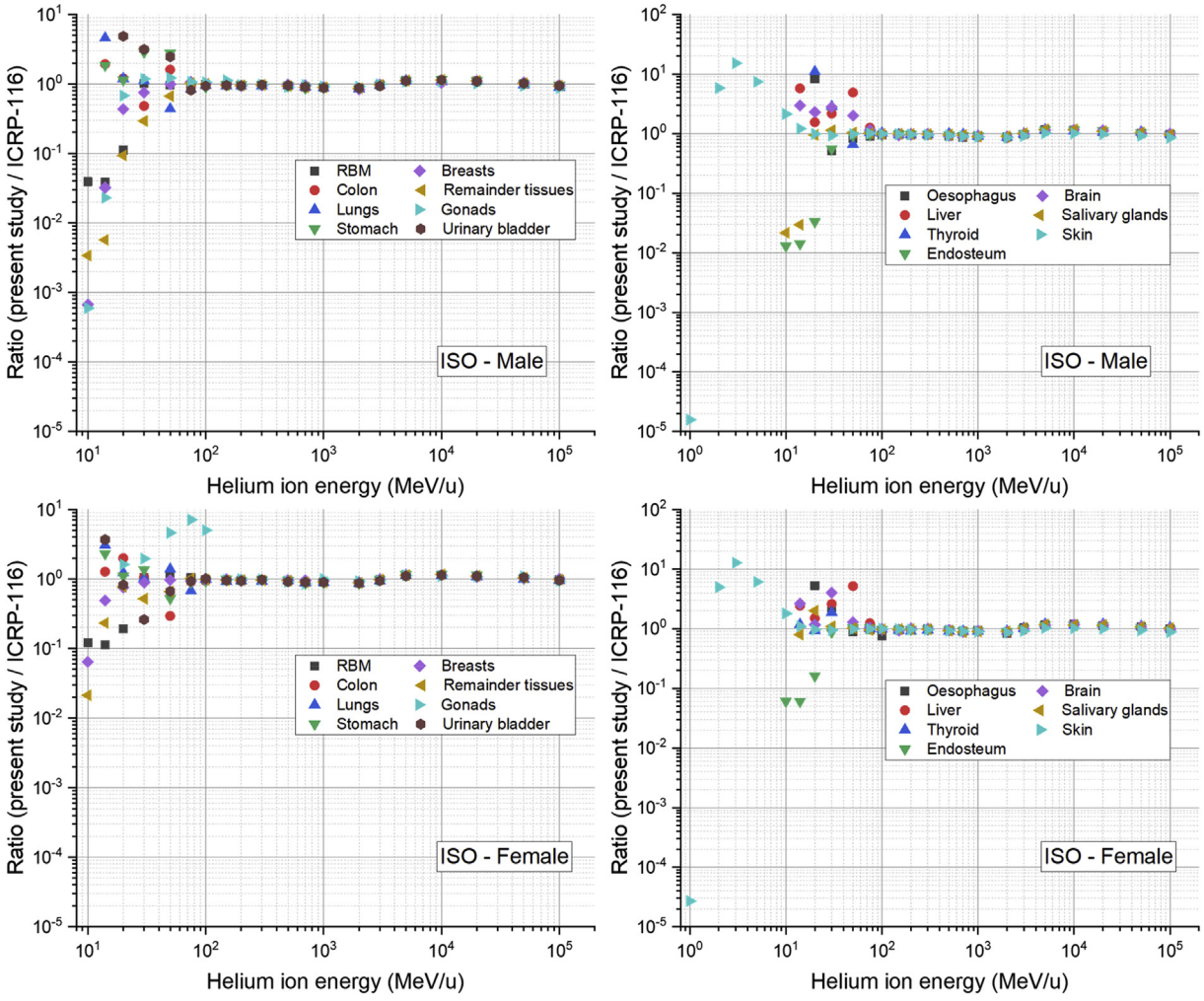

Fig. 9. Ratios of MRCP DC_T's calculated in present study to ICRP-116 DC_T's [5] for RBM, colon, lungs, stomach, breasts, remainder tissues, gonads, urinary bladder, oesophagus, liver, thyroid, endosteum, brain, salivary glands, and skin for helium ions in ISO geometry.

close to unity over the entire energy region in all the geometries (mostly between 0.8 and 1.2); that is, the MRCP DC_E's are generally similar to the ICRP-116 DC_E's. This observation can be easily expected by that the MRCP DC_T's overall agree with the ICRP-116 DC_T's as shown in Fig. 7. For protons, the MRCP DC_E's are also overall similar to the ICRP-116 DC_E's at energies >10 MeV, while significant differences are seen at lower energies. At energies $\leq$1.5 MeV, the MRCP DC_E's are lower by up to about eight orders of magnitude at the lateral geometries. At higher energies, on the other hand, the MRCP DC_E's are greater by up to about an order of magnitude at all the geometries. The result for helium ions shows a similar trend to that for protons; that is, MRCP DC_E's are generally similar to the ICRP-116 DC_E's at energies >10 MeV/u but significantly different at lower energies. The significant differences from the ICRP-116 DC_E's for both protons and helium ions are largely associated with the differences between the MRCP skin DC_T's and ICRP-116 skin DC_T's due to the use of the skin sensitive region defined in the MRCPs.

4. Conclusion

In the present study, we established a comprehensive dataset of DCs for external exposures of neutrons, protons, and helium ions by conducing Monte Carlo dose calculations using the MRCPs recently developed by the ICRP to address the limitations of the ICRP-110 VRCPs. The dataset includes the DC_T's for 30 individual organs/tissues and DC_E's, covering all the energies and irradiation geometries considered in ICRP *Publication* 116 [5]. The dosimetric improvement of the MRCPs over the VRCPs was investigated by comparing the MRCP DCs with the ICRP-116 DCs. We found that the MRCP DCs are generally similar to the ICRP-116 DCs for neutrons but there are significant differences up to several orders of magnitude for protons and helium ions due to the improved representation of the organs and tissues in the MRCPs. According to the results of the present study as well as the previous study [7] about photons and electrons, it can be concluded that for external exposures, the MRCPs provide similar doses to the VRCPs for penetrating radiations such as neutrons and γ rays, but different doses for weakly penetrating radiations such as beta and alpha particles. Most external exposure scenarios for radiation protection are concerned mainly with penetrating radiations, in which the use of the current ICRP-116 DCs based on the VRCPs is considered valid. In case of exposure scenarios involving weakly penetrating radiations, however, one should be aware of the presence of significant deviations of the ICRP-116 DCs from the MRCP DCs.

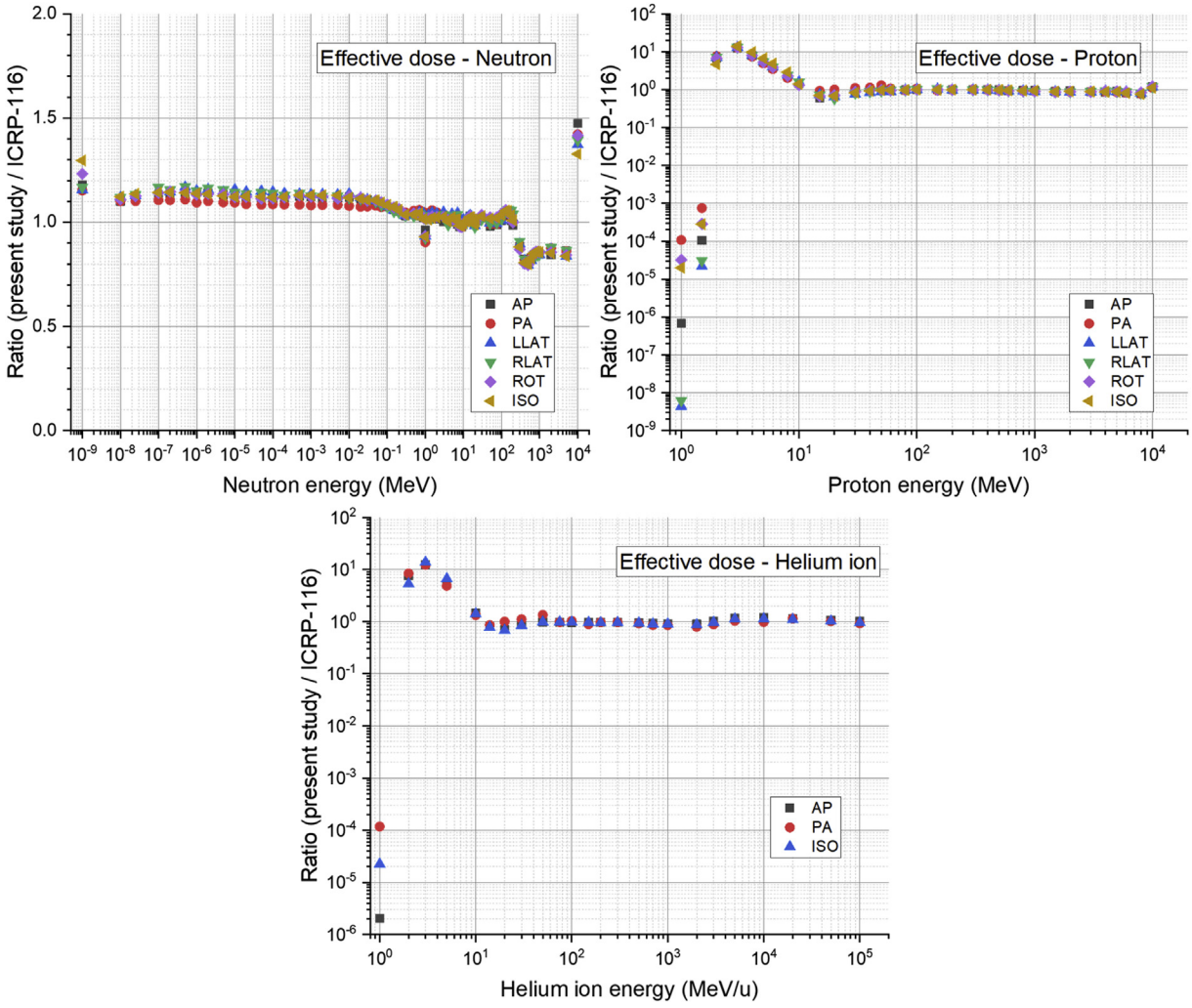

Fig. 10. Ratios of MRCP DC_E's calculated in present study to ICRP-116 DC_E's [5] for neutrons (upper left), protons (upper right), and helium ions (lower).

Acknowledgments

This project was supported by the Nuclear Safety Research Development (NSR&D) Program through Korea Foundation of Nuclear Safety (KOFONS), funded by the Nuclear Safety and Security Commission, and additionally, by the National Research Foundation of Korea funded by the Ministry of Science, ICT and Future Planning through the National Research Foundation of Korea (Project Nos.: 1705006, 2016R1D1A1A09916337). The work was also funded by the intramural program of the National Institutes of Health, National Cancer Institute, Division of Cancer Epidemiology and Genetics. One of the authors (Yeon Soo Yeom) was supported by a grant of the Korean Health Technology R&D Project through the Korean Health Industry Development Institute (KHIDI), funded by the Ministry of Health & Welfare, Republic of Korea (Project No: H18C2257). Two of the authors (Chansoo Choi and Haegin Han) were supported by the Global PhD Fellowship program (Project Nos.: NRF-2017H1A2A1046391, NRF-2018H1A2A1059767). The calculations in this work were performed on the National Institutes of Health's High-Performance Computing Biowulf cluster (http://hpc.nih.gov).

Appendix A. Supplementary data

Supplementary data to this article can be found online at https://doi.org/10.1016/j.net.2019.12.020.

References

[1] ICRP, Adult reference computational phantoms, ICRP Publ. 110 Ann ICRP 39 (2009) 1–166.
[2] C.H. Kim, Y.S. Yeom, T.T. Nguyen, M.C. Han, C. Choi, H. Lee, H. Han, B. Shin, J.-K. Lee, H.S. Kim, M. Zankl, N. Petoussi-Henss, W.E. Bolch, C. Lee, B.S. Chung, R. Qiu, K. Eckerman, New mesh-type phantoms and their dosimetric applications, including emergencies, Ann. ICRP 47 (2018) 45–62, https://doi.org/10.1177/0146645318756231.
[3] ICRP, Human respiratory tract model for radiological protection : a report of a Task Group of the international commission on radiological protection, ICRP Publ. 66 Ann ICRP. 23 (1994) 1–482.
[4] ICRP, Human alimentary tract model for radiological protection, ICRP Publ. 100 Ann ICRP. 36 (2006), https://doi.org/10.1016/j.icrp.2006.03.004, 1–336.
[5] ICRP, Conversion coefficients for radiological protection quantities for external radiation exposures, ICRP Publ. 116 Ann ICRP. 40 (2010) 1–258.
[6] ICRP, The ICRP computational framework for internal dose assessment for reference adults: specific absorbed fractions, ICRP Publ. 133 Ann ICRP. 45 (2016) 1–74.
[7] Y.S. Yeom, C. Choi, H. Han, H. Lee, B. Shin, T.T. Nguyen, M.C. Han, C. Lee, C.H. Kim, Dose coefficients of mesh-type ICRP reference computational phantoms for idealized external exposures of photons and electrons, Nucl. Eng. Technol. 51 (2019) 843–852, https://doi.org/10.1016/j.net.2018.12.006.
[8] J. Allison, K. Amako, J. Apostolakis, P. Arce, M. Asai, T. Aso, E. Bagli, A. Bagulya, S. Banerjee, G. Barrand, B.R. Beck, A.G. Bogdanov, D. Brandt, J.M.C. Brown, H. Burkhardt, Ph Canal, D. Cano-Ott, S. Chauvie, K. Cho, G.A.P. Cirrone, G. Cooperman, M.A. Cortés-Giraldo, G. Cosmo, G. Cuttone, G. Depaola, L. Desorgher, X. Dong, A. Dotti, V.D. Elvira, G. Folger, Z. Francis, A. Galoyan, L. Garnier, M. Gayer, K.L. Genser, V.M. Grichine, S. Guatelli, P. Guèye,

P. Gumplinger, A.S. Howard, I. Hřivnáčová, S. Hwang, S. Incerti, A. Ivanchenko, V.N. Ivanchenko, F.W. Jones, S.Y. Jun, P. Kaitaniemi, N. Karakatsanis, M. Karamitros, M. Kelsey, A. Kimura, T. Koi, H. Kurashige, A. Lechner, S.B. Lee, F. Longo, M. Maire, D. Mancusi, A. Mantero, E. Mendoza, B. Morgan, K. Murakami, T. Nikitina, L. Pandola, P. Paprocki, J. Perl, I. Petrović, M.G. Pia, W. Pokorski, J.M. Quesada, M. Raine, M.A. Reis, A. Ribon, A. Ristić Fira, F. Romano, G. Russo, G. Santin, T. Sasaki, D. Sawkey, J.I. Shin, I.I. Strakovsky, A. Taborda, S. Tanaka, B. Tomé, T. Toshito, H.N. Tran, P.R. Truscott, L. Urban, V. Uzhinsky, J.M. Verbeke, M. Verderi, B.L. Wendt, H. Wenzel, D.H. Wright, D.M. Wright, T. Yamashita, J. Yarba, H. Yoshida, Recent developments in Geant4, Nucl. Instrum. Methods Phys. Res. Sect. Accel. Spectrometers Detect. Assoc. Equip. 835 (2016) 186–225, https://doi.org/10.1016/j.nima.2016.06.125.

[9] Y.S. Yeom, J.H. Jeong, M.C. Han, C.H. Kim, Tetrahedral-mesh-based computational human phantom for fast Monte Carlo dose calculations, Phys. Med. Biol. 59 (2014) 3173–3185, https://doi.org/10.1088/0031-9155/59/12/3173.

[10] ICRP, The 2007 recommendations of the international commission on radiological protection, ICRP Publ. 103 Ann ICRP. 37 (2007) 1–332.

[11] Y.S. Yeom, Z.J. Wang, T.T. Nguyen, H.S. Kim, C. Choi, M.C. Han, C.H. Kim, J.K. Lee, B.S. Chung, M. Zankl, N. Petoussi-Henss, W.E. Bolch, C. Lee, Development of skeletal system for mesh-type ICRP reference adult phantoms, Phys. Med. Biol. 61 (2016) 7054–7073, https://doi.org/10.1088/0031-9155/61/19/7054.